Vietnam Journal of Earth Sciences, 45(3), 326-337, https://doi.org/ 10.15625/2615-9783/18461

Vietnam Journal of Earth Sciences
https://vjs.ac.vn/index.php/jse

A balanced edge detector for aeromagnetic data

Vinicius Theobaldo Jorge[1], Saulo Pomponet Oliveira[2,*], Luan Thanh Pham[3], Van-Hao Duong[4]

[1]*Graduate Program in Geology, Federal University of Paraná, Curitiba, Brazil*
[2]*Department of Mathematics, Federal University of Paraná, Curitiba, Brazil*
[3]*University of Science, Vietnam National University, Hanoi, Vietnam*
[4]*VNU School of Interdisciplinary Studies, Vietnam National University, Hanoi, Vietnam*

Received 02 March 2023; Received in revised form 23 April 2023; Accepted 26 June 2023

ABSTRACT

One of the most significant challenges in interpreting magnetic data is to mitigate the influence of the magnetization direction in the shape of the anomalies, especially when reduction to the pole fails to position them over the sources. We propose a balanced high-order filter that has low sensitivity to the direction of the resultant magnetization. We consider an edge-detector filter based on directional analytic signals of the vertically-integrated anomaly field. To ensure that anomalies from shallow and deep sources are equalized, we balance this filter with the magnitude of its two-dimensional Hilbert transform. The proposed filter is tested using aeromagnetic data from Apiaí Terrane, Southern Brazil. The enhanced map is highly correlated with the study area's NE-SW trend of geological structures. Our results highlight the importance of using the directional analytical signals, which help reduce the influence of the magnetization direction, and the balancing filters, for equalizing the signal of shallow and deep causative sources.

Keywords: Aeromagnetic data, enhancement filters, magnetization direction, directional analytic signal, Southern Brazil.

1. Introduction

Processing aeromagnetic data involves a variety of techniques that aid interpretation. A typical processing step uses enhancement methods such as reduction to the pole (RTP, Baranov and Naudy, 1964), which attempts to provide a transformed anomaly with vertical magnetization. Ideally, anomaly peaks would be located over the centers of the sources. However, this method suffers severe instability at low latitudes (Li, 2008). Moreover, sophisticated methods are usually needed to determine the resultant magnetization direction under remanent magnetization (Fedi et al., 1994; Dannemiller and Li, 2006). In particular cases, such as two-dimensional sources, RTP may be avoided by a suitable decomposition of the anomalous field (de Souza et al., 2020).

Another classical approach that reduces the influence of the magnetization direction is the analytical signal amplitude (AS, Nabighian, 1972; Roest et al., 1992), which does not suffer from the deficiencies of RTP but on the other hand, it is not independent on the magnetization direction in the 3D case (Li, 2006). It produces low-signal transformed anomalies in the case of deep sources (Cooper, 2009).

*Corresponding author, Email: saulopo@ufpr.br

In addition to the lower dependence on the magnetization direction, a relevant attribute of an enhancement filter is to accurately delineate the borders of the sources (Pham et al., 2021, 2022; Pham and Prasad, 2023). Among the recent contributions to edge detection, we highlight the works of Narayan et al. (2017, 2021), Melouah and Pham (2021), Melouah et al. (2021a, b), Sahoo et al. (2022), Kumar et al. (2018, 2022) and Kamto et al., 2023.

In this work, we propose a method that addresses the above issues and constitutes an efficient edge detector. Firstly, we consider a modified version of the edge detector filter of Beiki (2010) based on the vertical integration of the total field anomaly. The resulting map, mED, is less dependent on the magnetization direction than AS. Afterward, we compute the vertical derivative of mED and mED_z, and balance the amplitude of mED_z proceeding as Cooper (2009).

The proposed filter is thus a balanced vertical derivative of the modified directional analytic signal edge detector, denoted as mED_zASB. The filter mED_zASB is compared with both AS and its balanced version (Cooper, 2009) in synthetic data and in aeromagnetic data from Apiaí Terrane, Southern Brazil. These results reveal that the mED_z can more effectively centralize the anomaly over the sources than AS. Moreover, the selected amplitude balancing based on the 2D Hilbert transform can equalize anomalies from shallow and deep causative sources without significant noise amplification.

2. Theory

Let us initially consider the edge-detection filter proposed by Beiki (2010):

$$|ED| = \sqrt{\left[\frac{\partial}{\partial_z}\sqrt{g_{xx}^2 + g_{xy}^2 + g_{xz}^2}\right]^2 + \left[\frac{\partial}{\partial_z}\sqrt{g_{xy}^2 + g_{yy}^2 + g_{yz}^2}\right]^2}, \quad (1)$$

where g is the magnetic potential (Blakely, 1995, p. 328), and sub-indices x, y, and z denote partial derivatives. We employ a modified version of |ED| where the magnetic potential is replaced with the vertical integral F of the total-field anomaly f:

$$mED = \sqrt{\left[\frac{\partial}{\partial_z}\sqrt{F_{xx}^2 + F_{xy}^2 + F_{xz}^2}\right]^2 + \left[\frac{\partial}{\partial_z}\sqrt{F_{xy}^2 + F_{yy}^2 + F_{yz}^2}\right]^2}. \quad (2)$$

Since $F_z = f$, some terms in Eq. (2) can be simplified: $F_{xz} = f_x$ and $F_{yz} = f_y$. Moreover, as $\Delta f = 0$, we can compute mED using only x– and y–derivatives of f and its vertical derivative f_z. For instance, the first expression under the square in equation 2 can be written as follows:

$$\frac{\partial}{\partial_z}\sqrt{F_{xx}^2 + F_{xy}^2 + F_{xz}^2} = \frac{F_{xx}F_{xxz} + F_{xy}F_{xyz} + f_x f_{xz}}{\sqrt{F_{xx}^2 + F_{xy}^2 + f_x^2}} = \frac{F_{xx}f_{xx} + F_{xy}f_{xy} + f_x f_{zx}}{\sqrt{F_{xx}^2 + F_{xy}^2 + f_x^2}}. \quad (3)$$

Thus, the mED can be written as follows:

$$mED = \sqrt{\frac{(F_{xx}f_{xx} + F_{xy}f_{xy} + f_x f_{zx})^2}{F_{xx}^2 + F_{xy}^2 + f_x^2} + \frac{(F_{xy}f_{xy} + F_{yy}f_{yy} + f_y f_{zy})^2}{F_{xy}^2 + F_{yy}^2 + f_y^2}}. \quad (4)$$

We have found that the vertical derivative of mED, calculated in the frequency domain (Pham et al., 2021), is an excellent edge detector. However, the amplitude of mED_z significantly decays in the presence of deep sources. For this reason, we apply to mED_z the same balancing strategy as in the balanced analytic signal filter (Cooper, 2009). The resulting method is given as follows:

$$mEDzASB = \frac{mED_z}{k+\sqrt{(H_x[mED_z])^2+(H_y[mED_z])^2+(mED_z)^2}}, \quad (5)$$

where ($H_x[\cdot]$, $H_y[\cdot]$) is the 2D Hilbert transform, which can be defined in the frequency domain as

$$\left(\widehat{H}_x[f](u,v), \widehat{H}_y[f](u,v)\right) = \left(\frac{-iu\hat{f}(u,v)}{\sqrt{u^2+v^2}}, \frac{-iv\hat{f}(u,v)}{\sqrt{u^2+v^2}}\right), \quad (6)$$

and k is a parameter that controls the amplitude balance. We have chosen k = 0, as Cooper (2009) suggested. A flow chart of the entire process is shown in Fig. 1.

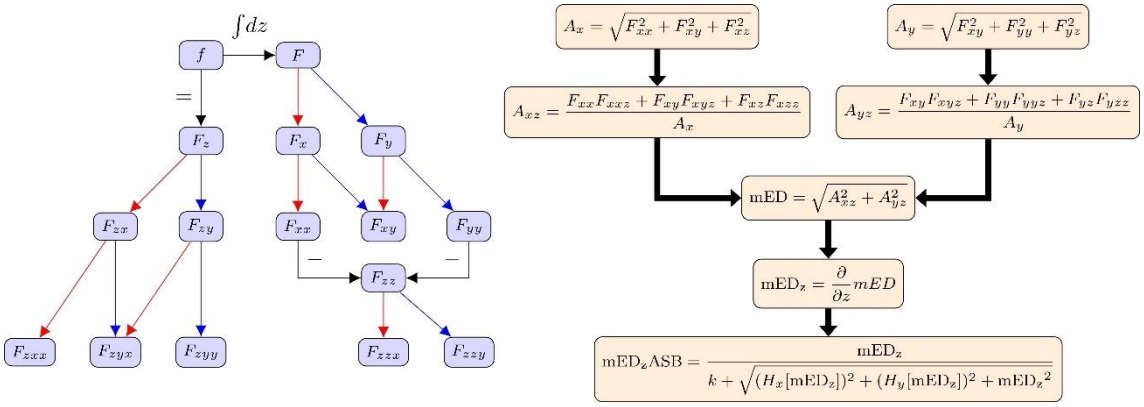

Figure 1. Flow chart of the mEDzASB method. Red arrows and blue arrows denote differentiation to x and y, respectively. The differentiation order does not change the function (e.g., F_{xz}=F_{zx})

3. Results and discussion

In the following, we present and discuss some experiments with synthetic and real data to illustrate the proposed method. For comparison purposes, in addition to mED_z and mED_zASB, we also show the results using the analytic signal amplitude (Roest et al., 1992)

$$AS = \sqrt{f_x^2 + f_y^2 + f_z^2} \quad (7)$$

and the balanced analytic signal amplitude (Cooper, 2009)

$$ASB = \frac{AS}{k+\sqrt{(H_x[AS])^2+(H_y[AS])^2+AS^2}}. \quad (8)$$

To cope with noise generated by the high-order derivatives or the balancing filter, we compute the vertical derivative using the β-VDR method with parameter β = 30 in all calculations. This method uses a finite difference formula where all terms are subjected to upward continuation without losing approximation accuracy (Oliveira and Pham, 2022). On the other hand, derivatives in x- and y- directions are calculated using finite differences in the space domain.

3.1. Synthetic data

We consider a model comprising three prismatic sources of the same size (Fig. 2a). The parameters of the sources are presented in Table 1.

Table 1. Parameters of the synthetic example

Parameter	M1	M2	M3
x-coordinates of center (km)	50	100	150
y-coordinates of center (km)	150	100	50
Width (km)	40	40	40
Length (km)	40	40	40
Depth to top (km)	3	5	7
Depth to bottom (km)	6	8	10

The theoretical magnetic anomalies due to the sources were calculated as in Rao and Babu (1991) on a 201×201 square grid with a spacing of 1 km. For simplicity, we do not consider remanent magnetism, and all prisms

are under the same induced magnetization, whose value is 2.1 A/m. We set the declination and inclination as D = -20° and I = -35°, respectively, approximately the same as in the real data. The resulting total-field anomaly (TFA) is shown in Fig. 2b.

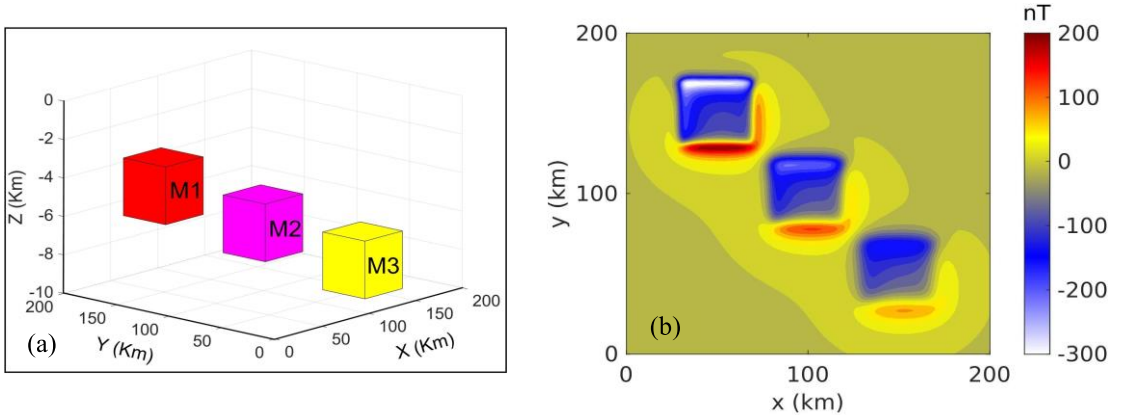

Figure 2. 3D view of the magnetic model (a) and TFA generated from the model in Fig. 2a (b)

The results are shown in Fig. 3. AS (Fig. 3a) and mED (Fig. 3b) have difficulties with the deeper body, although mED has a sharper result. For the balanced approaches (Figs. 3c-d), we can note the improvement obtained by the proposed method.

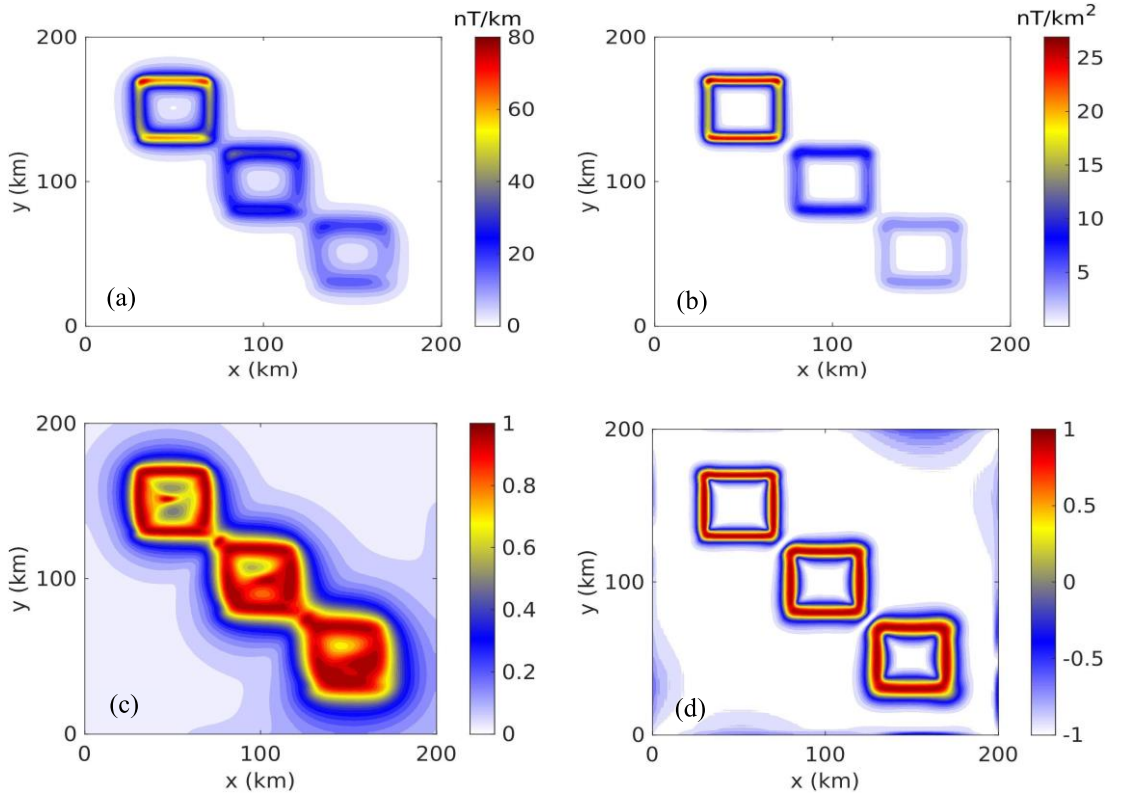

Figure 3. Results obtained from the data in Fig. 2b: (a) AS; (b) mED; (c) ASB; (d) mEDzASB

We have also considered the effect of additive noise in the synthetic experiments. Fig. 4 shows the TFA contaminated with Gaussian noise of amplitude equal to 1% of the maximum absolute value of the data. The noise effect over the magnetic anomaly can be seen in the contour line near 0 nT, while the effect on the transformed maps (Fig. 5) is widespread. However, the source edges remain visible in the mEDzASB map (Fig. 5d). Although our method is more noise-sensitive, it provided better results than the other applied methods. In the presence of a high noise level, upward-continued data can be used to reduce noise before the application of this method, as recommended by Hang et al. (2017) and Oksum et al. (2021).

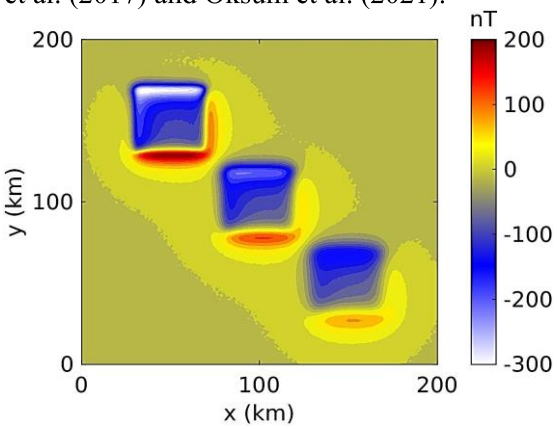

Figure 4. Data from Fig. 2b contaminated with Gaussian amplitude noise equal to 1% of the maximum data absolute value

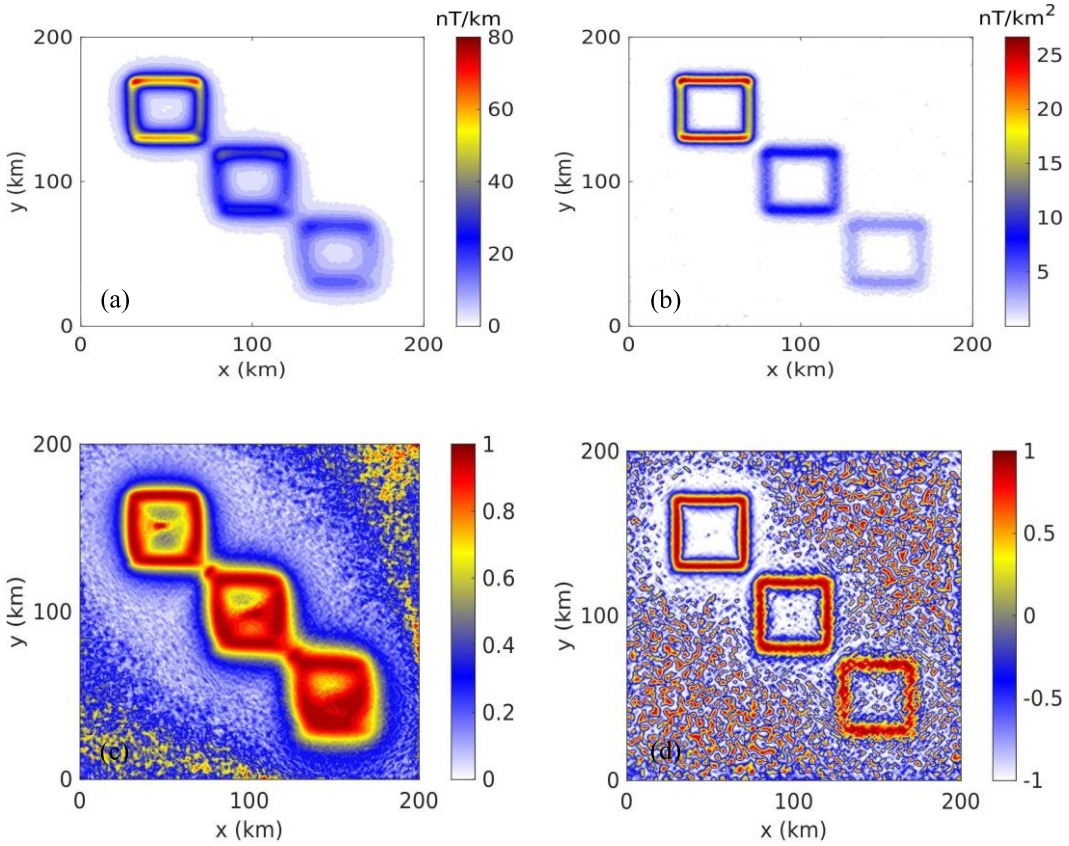

Figure 5. Results obtained from the data in Fig. 4: (a) AS; (b) mED; (c) ASB; (d) mEDzASB

3.2. Field data

To illustrate an application of the proposed method to real data, we selected a study area in the Apiaí Terrane, between the states of Paraná and São Paulo, in Southern Brazil (Fig. 6). The study area is delimited between longitudes 48°40' W and 48°30' W and longitudes 24°50' S and 25°00' S.

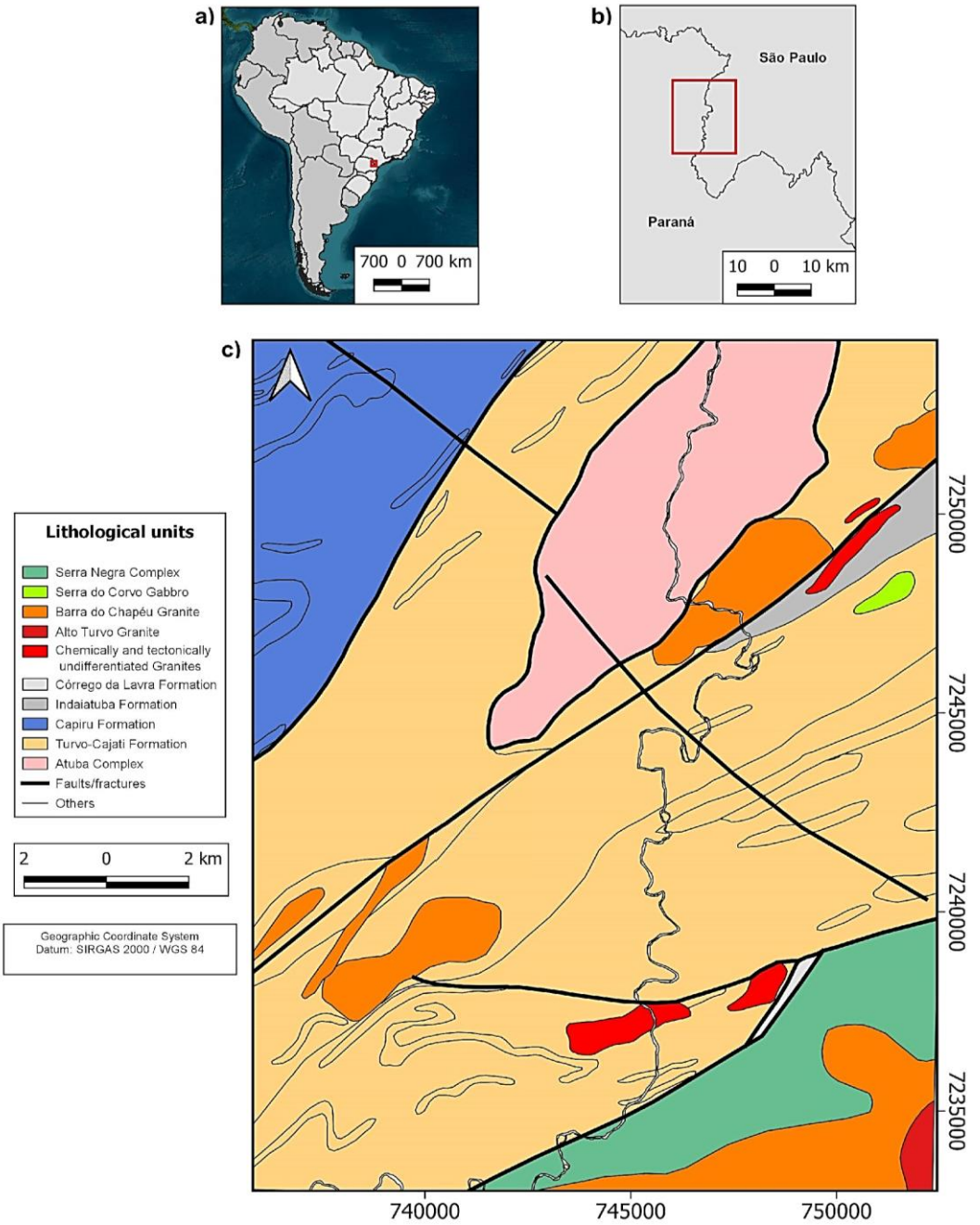

Figure 6. Location and geology of the study area: a) Location (red square) within Brazil, South America; b) Regional location between the states of Paraná and São Paulo, Brazil; c) Simplified geological map

A predominance of faults and fractures occurs preferentially in the NE-SW direction. There are also NW-directed discontinuities, which deviate from the regional structural pattern with a NE-SW direction. The rocks present a structural evolution evidenced by the superposition of events of several deformation phases, with intense deformation resulting from the low-angle thrust tectonics, and these events preferably have a NE-SW and NW-SE direction. The area has various lithological units, briefly described below (see Faleiros et al., 2012).

The Capiru Formation, from Tonian to Ediacaran age, is composed of metapelites (rhythmic phyllite, slate), marble, and mica schist. The metapelites are mainly composed of slate and phyllite (metasilicate and meta argillite), with fine lamination and sedimentary banding. The marble is presented in light gray color to white, in general calcarenite, with sedimentary bedding of centimetric to metric thickness. Finally, the mica-schist presents slightly more intense metamorphism and deformation and scarcity of intercalations of carbonate rocks. The Turvo-Cajati Formation, of Tonian to Ediacaran age, is constituted predominantly by thick migmatitic paragneisses and mica schists with a generally lenticularized and diffuse banding defined by the alternation between mesocratic beds formed by biotite, sillimanite and garnet, leucosomes formed by quartz, potassium feldspar and plagioclase and sillimanite subcentimeter bands. This unit is dominated by bodies of thin mica-schist or phyllite, dark gray, formed by biotite, muscovite, quartz, and chlorite, usually with porphyroblasts of disseminated millimeter garnet and, locally, staurolite.

The Atuba complex, from Riacian to Orosirian age, presents a single unit composed of two main lithotypes. One is related to a hornblende banded gneiss, formed by plagioclase, quartz, hornblende, epidote, chlorite, and biotite and the other consisting of fine gneiss, dark green, schist, composed of feldspar, quartz, biotite, hornblende, and chlorite. The Barra do Chapéu Granite, of Ediacaran age with dominant lithotype, consists of pink to gray porphyritic granite with mega crystals of pink alkaline feldspar. Isotropic and foliate terms occur. It consists of hornblende and biotite, representing the main mafic minerals, plagioclase and quartz.

From Archean to Paleoproterozoic age, the Serra Negra Complex is constituted by gneissic-granulitic rocks of basic composition, retro metamorphized in conditions of greenschist facies superior to amphibolite. The main lithotype consists of basic hornblende-gneiss, dark gray, fine to medium-grained, which may have foliation defined by the preferential orientation of the minerals, amphibolite bodies that alternate with thin layers and lenses, heterogeneously sheared, of phyllite, in addition to the iron formation in the magnetite facies.

The Indaiatuba Formation of the Ediacaran age is predominantly formed by rhythmic metapelite (slate), with centimeter sedimentary bedding and a violet to purple or porcelain color. The metapelite presents a well-marked sub-vertical slate cleavage subparallel to the sedimentary bedding and interbedded layers of whitish arcosean sandstone, with grains varying transitionally from coarse to fine. The Córrego da Lavra Formation, of Ediacaran age, is formed, essentially, by rhythmic silty-clay metapelite (slate) of gray to violet colors, with main foliation defined by crenulation cleavage with associated differentiated millimeter to submillimeter banding. The Alto Turvo Granite, of Ediacaran age, is composed of thick equigranular granite, isotrope, pink to slightly brownish, and minerals such as biotite and hornblende, titanite, zircon, and apatite. Chemically and tectonically indiscriminate granites of the Ediacaran age comprise

chemically and tectonically indiscriminate stocks and plutons of granitic rocks. The Serra do Corvo Gabbro, of Mesozoic age, also contains stocks of alkaline gabric rocks (olivine-gabbro) with dimensions smaller than 2 km in diameter.

To our knowledge, there are few geophysical studies about the Apiaí Terrane. Rosales et al. (2001) proposed a geological-geophysical map of the Apiaí Fold Belt based on interpreting Bouguer anomaly profiles. Faleiros et al. (2012) inferred the presence of sources with multiple shapes in the Apiaí Terrane based on magnetic and radiometric data. Castro and Ferreira (2015) studied structural models of the southern portion of the Ribeira Belt, which includes our study area, based on the integration of aeromagnetic data reduced to the pole, ground gravimetric surveys, and regional geological maps.

The Geological Survey of Brazil (2011) acquired the aeromagnetic data along north-south flight lines with 500 m spacing, with a mean terrain clearance of 100 m. The data were interpolated to a square grid with a spacing of 125 m using the minimum curvature method. Moreover, the data was subject to an upward continuation of 125 m. The resulting total-field anomaly is shown in Fig. 7.

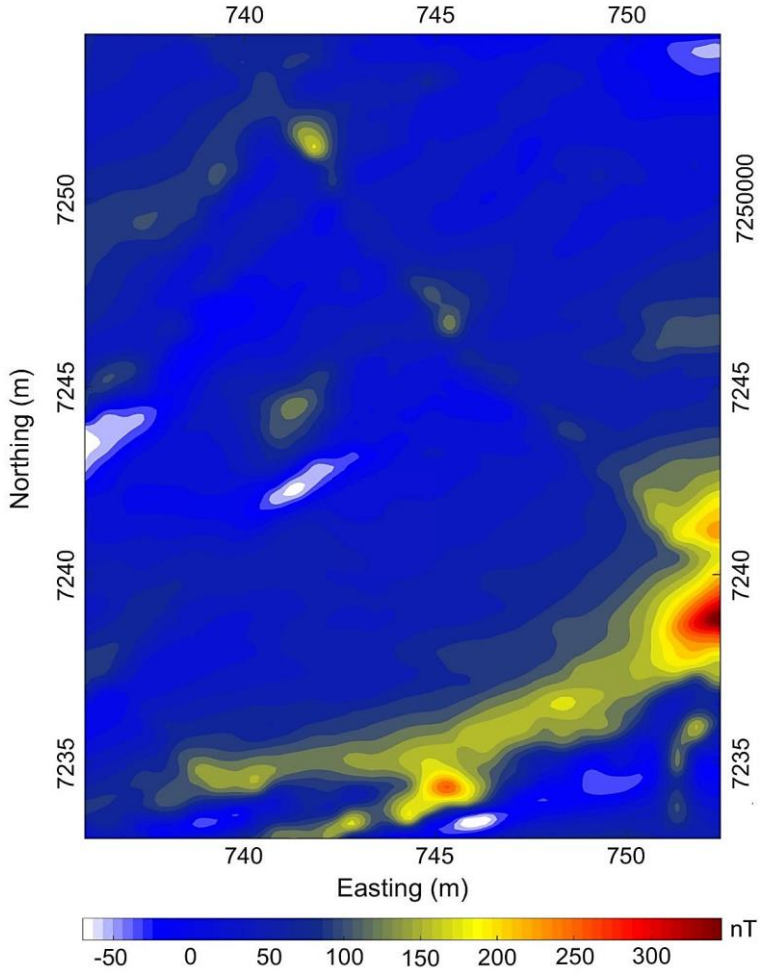

Figure 7. Total-field aeromagnetic data from the study area (Fig. 6c)

The results of the proposed and related filters are shown in Fig. 8. Similar to the synthetic data, the lack of amplitude equalization is an issue for both AS (Fig. 8a) and mED (Fig. 8b). As in Faleiros et al. (2012), the positive anomalies in the AS map are limited and disperse. For the balanced methods, ASB and mED$_z$ASB (Figs. 8c-d), the latter is more illustrative of the main features of the data.

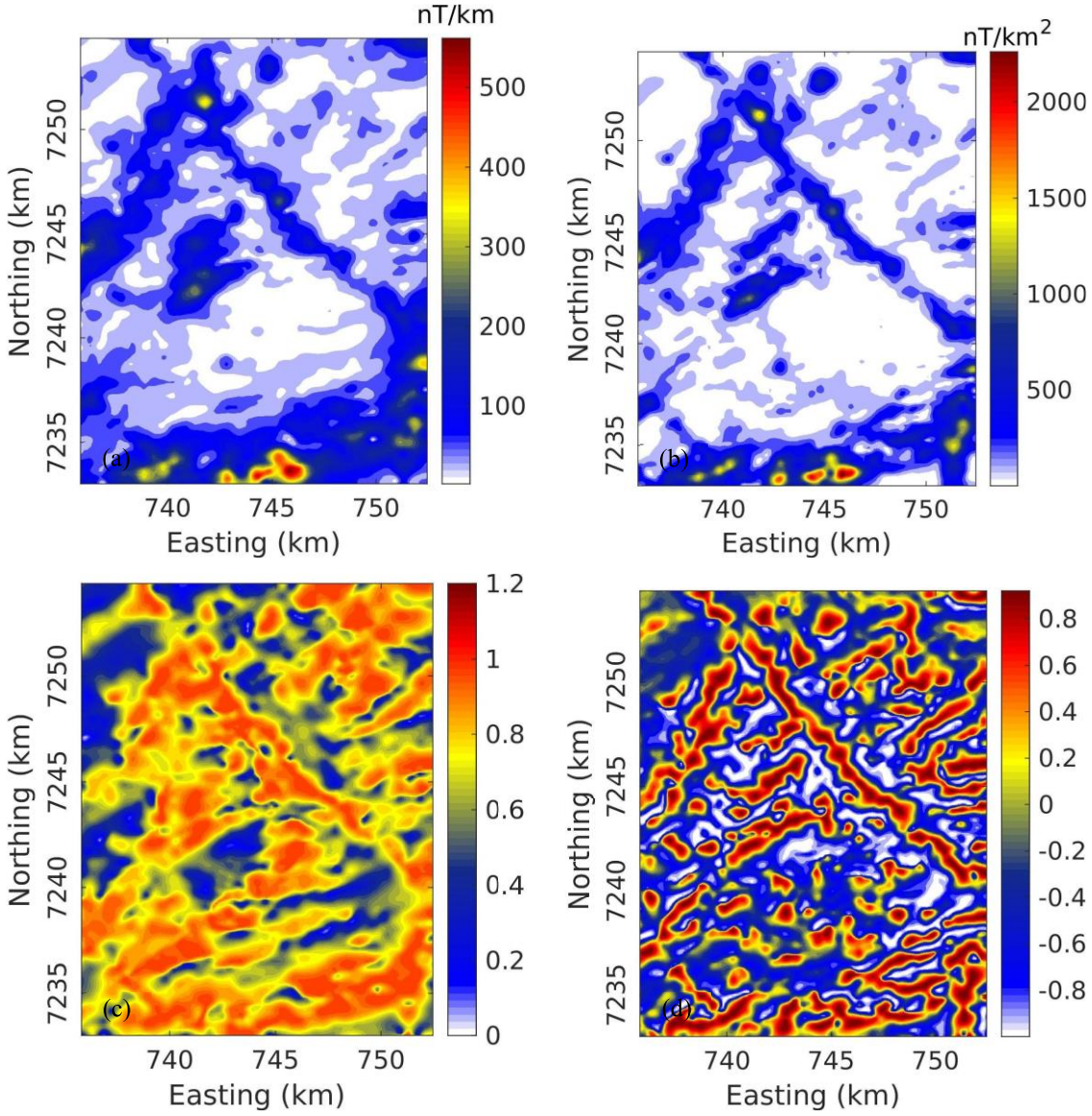

Figure 8. Results obtained from the data in Fig. 7: (a) AS; (b) mED; (c) ASB; (d) mEDzASB

4. Discussions

The presented method described in this paper uses a modified edge-detection (mED) filter introduced by Beiki (2010) and the balanced analytic signal proposed by Cooper (2009). Since the proposed method is based on directional analytical signals, reducing the influence of the magnetization direction is

helpful, especially when reduction to the pole or other methods fail to position them over the sources. On the other hand, our method balances the mED filter by using its orthogonal Hilbert transforms. Therefore it helps map the deep causative sources. The results obtained from the synthetic examples showed that our method is less dependent on the magnetization direction than other methods. In addition, the proposed method can provide more transparent and more accurate edges than other techniques. Figs. 3 and 5 show that the directional analytical signals preserve the shape of the sources, while the maps based on analytic signals are significantly deformed due to non-vertical magnetization. The disadvantage of the proposed technique is that it is more noise-sensitive than others. However, the upward continuation of the total-field anomaly can reduce the noise effect.

The practical application shows that the proposed filter is helpful in mapping a wide range of magnetic features in the Apiaí Terrane. In this sense, Fig. 9 compares the Signum transform (de Souza and Ferreira, 2012; Weihermann et al., 2018) of the mEDzASB map with the geologic map. The mEDzASB map (Fig. 8d) and its Signum transform (Fig. 9a) indicate the presence of trends in NE-SW and NW-SE directions, with the NE-SW trend predominating. The mEDzASB result clearly correlates well with the NE-SW trend of geological structures in the region (Fig. 9). The mapped NE-SW trending faults mostly match some of the transformed anomalies. In addition, the mEDzASB map also demonstrates the existence of two NW-SE trending faults and fractures in the geology map. However, more geophysical and geological data should still be combined for comprehensive interpretation in actual application.

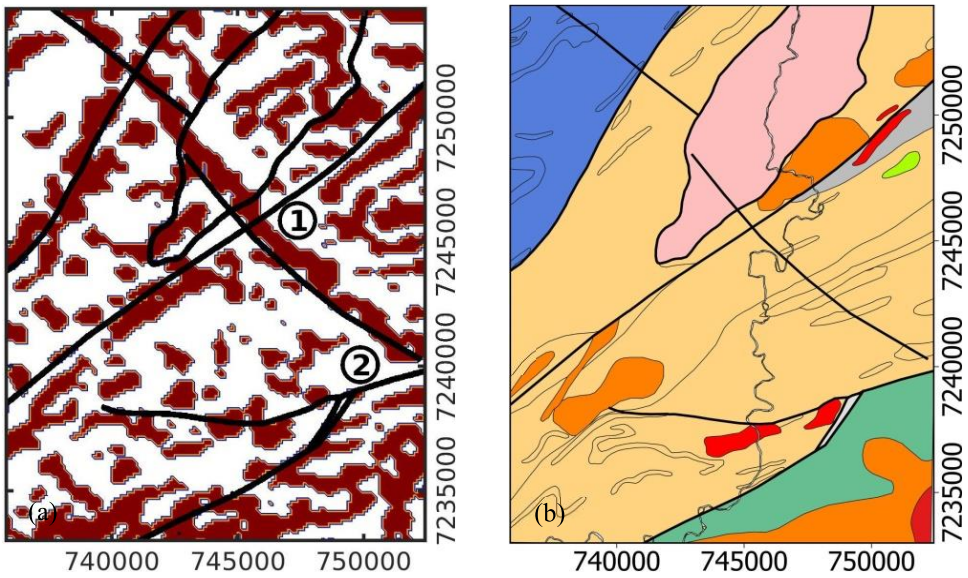

Figure 9. Interpretation of the results (a) obtained from the Signum transform of the data in Fig. 8d, considering the geological map (b). Labels (1) and (2) indicate the Putunã and Faxinal shear zones, respectively (Faleiros et al., 2012)

5. Conclusions

A novel filter, mEDzASB, has been introduced for interpreting magnetic data. Although this filter is a modified version of the ASB filter, it offers some improvements compared to the original version. The

proposed filter was tested on both synthetic and natural data. Compared with the other filters, it has shown to be more effective in identifying source locations without resorting to reduction to the pole and avoiding deformed anomalies in the 3D analytical signal amplitude. The disadvantage of the mEDzASB filter is that it is more noise-sensitive than filters. However, this problem can be solved by using an upward continuation of the total-field anomaly before applying the mEDzASB filter.

Acknowledgments

This study was financed in part by the Coordenação de Aperfeiçoamento de Pessoal de Nível Superior - Brazil (CAPES) - Finance Code 001, by National Council of Technological and Scientific Development (CNPq, Grant number 316376/2021-3), and by Ministry of Natural Resources and Environment, Vietnam under Grant Agreement No: TNMT.2022.02.20. Luan Thanh Pham was funded by Vingroup JSC and supported by the Postdoctoral Scholarship Programme of Vingroup Innovation Foundation (VINIF), Vingroup Big Data Institute (VinBigdata), code VINIF.2022.STS.43.

References

Baranov V., Naudy H., 1964. Numerical calculation of the formula of reduction to the magnetic pole. Geophysics, 29(1), 67-79.

Beiki M., 2010. Analytic signals of gravity gradient tensor and their application to estimate source location. Geophysics, 75(6), I59-I74.

Castro L.G.D., Ferreira F.J.F., 2015. Geophysical-structural framework of southern Ribeira Belt. Brazilian Journal of Geology, 45(4), 499-516, in Portuguese.

Cooper G.R.J., 2009. Balancing images of potential-field data. Geophysics, 74(3), L17-L20.

Dannemiller N., Li Y., 2006. A new method for determination of magnetization direction. Geophysics, 71(6), L69-L73.

De Souza J., Ferreira F.J.F., 2012. On the use of derivatives for interpreting magnetic anomalies due to dyke-like bodies: Qualitative and quantitative analysis. In: Istanbul 2012-International Geophysical Conference and Oil & Gas Exhibition. Society of Exploration Geophysicists, 1-4.

De Souza J., Oliveira S.P., Ferreira F.J.F., 2020. Using parity decomposition for interpreting magnetic anomalies from dikes having arbitrary dip angles, induced and remanent magnetization. Geophysics, 85(3), J51-J58.

Faleiros F.M., Morais S.M., Costa V.S., 2012. Geology and mineral resources of the Apiaí sheet - SG.22-X-B-V - states of São Paulo e Paraná (Scale 1:100.000). Tech. rep., Geological Survey of Brazil, in Portuguese.

Fedi M., Florio G., Rapolla A., 1994. A method to estimate the total magnetization direction from a distortion analysis of magnetic anomalies. Geophysical Prospecting, 42(3), 261-274.

Geological Survey of Brazil, 2011. Aerogeophysical project Paraná-Santa Catarina: survey and processing of magnetometric and gamma-ray spectrometric data. Tech. rep., Lasa Prospecções, in Portuguese.

Hang N.T., Thanh D.D., Minh L.H., 2017. Application of directional derivative method to determine boundary of magnetic sources by total magnetic anomalies. Vietnam J. Earth Sci., 39(4), 360-375.

Kamto P.G, Oksum E., Pham L.T., Kamguia J., 2023. Contribution of advanced edge detection filters for the structural mapping of the Douala Sedimentary Basin along the Gulf of Guinea. Vietnam Journal of Earth Sciences. https://doi.org/10.15625/2615-9783/18410

Kumar U., Pal S.K., Sahoo S.D., Narayan S., Saurabh S. M., Ganguli S.S., 2018 Lineament mapping over Sir Creek ofshore its surroundings using high resolution EGM2008 gravity data: an integrated derivative approach. Journal of the Geological Society of India, 91, 671-678.

Kumar U., Narayan S., Pal S.K., 2022. Structural and tectonic interpretation of EGM2008 gravity data around the Laccadive ridge in the Western Indian Ocean: An implication to continental crust. Geocarto International, 37(11), 3179-3198.

Li X., 2006. Understanding 3D analytic signal amplitude. Geophysics, 71(2), L13-L16.

Li X., 2008. Magnetic reduction-to-the-pole at low latitudes: Observations and considerations. The Leading Edge, 27(8), 990-1002.

Melouah O., Eldosouky A.M., Ebong E.D., 2021a. Crustal architecture, heat transfer modes and geothermal energy potentials of the Algerian Triassic provinces. Geothermics, 96, 102211.

Melouah O., Pham L.T., 2021. An improved ILTHG method for edge enhancement of geological structures: application to gravity data from the Oued Righ valley. Journal of African Earth Sciences, 177, 104162.

Melouah O., Steinmetz R.L.L., Ebong E.D., 2021. Deep crustal architecture of the eastern limit of the West African Craton: Ougarta Range and Western Algerian Sahara. Journal of African Earth Sciences, 183, 104321.

Nabighian M.N., 1972. The analytic signal of two-dimensional magnetic bodies with polygonal cross-section: its properties and use for automated anomaly interpretation. Geophysics, 37(3), 507-517.

Narayan S., Sahoo S.D., Pal S.K., Kumar U., Pathak V.K., Majumdar T.J., Chouhan A., 2017. Delineation of structural features over a part of the Bay of Bengal using total and balanced horizontal derivative techniques. Geocarto International, 32(4), 351-366.

Narayan S., Kumar U., Pal S.K., Sahoo S.D., 2021. New insights into the structural and tectonic settings of the Bay of Bengal using high-resolution earth gravity model data. Acta Geophysica, 69, 2011-2033.

Oksum E., Le D.V., Vu M.D., Nguyen T.H.T., Pham L.T., 2021. A novel approach based on the fast sigmoid function for interpretation of potential field data. Bulletin of Geophysics and Oceanography, 62, 543-556.

Oliveira S.P., Pham L.T., 2022. A stable finite difference method based on upward continuation to evaluate vertical derivatives of potential field data. Pure and Applied Geophysics, 179(12), 4555-4566.

Pham L.T., Oksum E., Duc T., Vu M.D., 2021. Comparison of different approaches of computing the tilt angle of the total horizontal gradient and tilt angle of the analytic signal amplitude for detecting source edges. Bulletin of the Mineral Research and Exploration, 163, 53-62.

Pham L.T., Eldosouky A.M., Melouah O., Abdelrahman K., Alzahrani H., Oliveira S.P., Andráš P., 2021. Mapping subsurface structural lineaments using the edge filters of gravity data. Journal of King Saud University-Science, 33(8), 101594.

Pham L.T., Oksum E., Kafadar O., Trinh P.T., Nguyen D.V., Vo Q.T., Le S.T., Do T.D., 2022. Determination of subsurface lineaments in the Hoang Sa islands using enhanced methods of gravity total horizontal gradient. Vietnam J. Earth Sci., 44(3), 395-409.

Pham L.T., Prasad K.N.D., 2023. Analysis of gravity data for extracting structural features of the northern region of the Central Indian Ridge. Vietnam J. Earth Sci., 45(2), 147-163.

Rao D.B., Babu N.R., 1991. A rapid method for three-dimensional modeling of magnetic anomalies. Geophysics, 56(11), 1729-1737.

Roest W.R., Verhoef J., Pilkington M., 1992. Magnetic interpretation using the 3-D analytic signal. Geophysics, 57(1), 116-125.

Rosales M.J.T., Shukowsky W., Mantovani M.S.M., 2001. Geophysical study on the structural geological context of the Apiaí Belt, Southwest São Paulo, Brazil. In: 7th International Congress of the Brazilian Geophysical Society, Brazilian Geophysical Society, in Portuguese, 474-477.

Sahoo S., Narayan S., Pal S.K., 2022. Fractal analysis of lineaments using CryoSat-2 and Jason-1 satellite-derived gravity data: Evidence of a uniform tectonic activity over the middle part of the Central Indian Ridge. Physics and Chemistry of the Earth, 128, 103237.

Weihermann J.D., Ferreira F.J.F., Oliveira S.P., Cury L.F., De Souza J., 2018. Magnetic interpretation of the Paranaguá terrane, southern Brazil by signum transform. Journal of Applied Geophysics, 154, 116-127.